Provided for non-commercial research and education use.
Not for reproduction, distribution or commercial use.

This article appeared in a journal published by Elsevier. The attached copy is furnished to the author for internal non-commercial research and education use, including for instruction at the authors institution and sharing with colleagues.

Other uses, including reproduction and distribution, or selling or licensing copies, or posting to personal, institutional or third party websites are prohibited.

In most cases authors are permitted to post their version of the article (e.g. in Word or Tex form) to their personal website or institutional repository. Authors requiring further information regarding Elsevier's archiving and manuscript policies are encouraged to visit:

http://www.elsevier.com/copyright

Author's personal copy

Simulation Modelling Practice and Theory 19 (2011) 133–147

Contents lists available at ScienceDirect

Simulation Modelling Practice and Theory

journal homepage: www.elsevier.com/locate/simpat

Two-level control strategy of an eight link biped walking model

Andrej Olenšek *, Zlatko Matjačić

University Rehabilitation Institute, Republic of Slovenia, Linhartova 51, 1000 Ljubljana, Slovenia

ARTICLE INFO

Article history:
Received 21 April 2009
Received in revised form 28 May 2010
Accepted 31 May 2010
Available online 8 June 2010

Keywords:
Push off
Within-step control
Between-step control

ABSTRACT

This paper presents an adaptive two-level control strategy for a biped walking model and demonstrates its performance in a wide range of walking modes with considerably diverse model and control parameter settings. Proposed control strategy inherits a push off that resembles considerably to forceful extension of the trailing leg during push off in human locomotion and represents a very important source of forward propulsion. Extensive simulations have shown that adjustments in the push off related parameter on higher between-step control level after each step enable evolution of various walking modes of the biped walker at selected walking speeds and distinctive gait patterns. It also allows us to investigate the changes in gait kinematics and kinetics of the biped walking model due to changes in gait velocity, torso inclination and propulsion distribution profiles.

© 2010 Elsevier B.V. All rights reserved.

1. Introduction

Even though biomechanics of human locomotion is well understood [28,29] and is instrumented gait analysis becoming an indispensable tool in human locomotion analyses, successful therapeutical intervention in clinical gait assessment depends predominantly on our ability to correctly interpret recorded gait kinematics and kinetics. In this sense the benefits of instrumented gait analysis can only be partially exploited, as we can only to some extent assert the state of biomechanical structure, but cannot use the data in subsequent predictions of the most appropriate therapeutical intervention as well. Only recently a promising support to instrumented gait analysis has been noted in robotics, where the possibility to investigate and to define characteristic walking pattern in a biped walking model for arbitrary variation of model and control parameter is the most obvious benefit.

Structural complexity of kinematic linkage and walking algorithms employed in biped walking models [1,4–6,17,19,21,24] or biped robots [3,10–13,18] considerably affect the degree of resemblance to human walking. The simplest biped mechanisms with only a few degrees of freedom are passive dynamic [3,21,12,13,27] and ballistic [10,16] robots. While passive dynamic robots are free from actuation and utilize inertial and gravitational forces to develop stable downhill walking, the ballistic walkers employ swing leg actuation only at the beginning and the end of the stance phase, with inertial and gravitational forces being utilized elsewhere. Due to partial or complete absence of actuation this class of biped machines exhibit considerable energy efficiency and minimal control efforts as well as naturally appearing movement, but simultaneously lacks the robustness and insensitivities to disturbances and considerably limits the maximal number of degrees of freedom.

On the other hand, trajectory tracking enables considerable human-like locomotion of the robot, where the set of trajectories being traced defines the configuration set of the walker. Reference trajectories are predetermined either through detailed human gait analyses constructed templates [1,4] or calculated through optimization of certain cost criteria [19,20,23],

* Corresponding author. Tel.: +386 1 4758 241; fax: +386 1 4372 070.
E-mail address: andrej.olensek@mail.ir-rs.si (A. Olenšek).

1569-190X/$ - see front matter © 2010 Elsevier B.V. All rights reserved.
doi:10.1016/j.simpat.2010.05.017

Author's personal copy

whereas the stability is subject to zero-moment point (ZMP) control [15,22]. While producing realistic human-like movements, the necessity for a priory determination of reference trajectories imposes a significant drawback, for being able to generate and investigate versatile characteristic gait pattern subject to model parameter variations would be preferable.

We can overcome this drawback by applying feedback control [5,6,30,31] into biped walking model and robot. Encoding elementary walking premises as a set of scalar-valued output functions that are fed back to the controller via feedback control was proposed by Grizzle [5,6]. In five degrees of freedom walking model he formally proved asymptotic stability of the controller, if all scalar-valued output functions were expressed as functions of stance leg angle with respect to vertical. However even in simple models control efforts in feedback control of biped walker are immense and magnify considerably in models with many degrees of freedom. For this reason the majority of feedback control based models in the literature has simple structure with only a few degrees of freedom and assumes instantaneous transition from single support to swing phase. The absence of double support is a significant simplification which prevents restitution of lost energy at the impact of swing leg with the ground in a similar way as in human locomotion. Biomechanical studies have revealed that the majority of power generation occurs during forceful extension of the trailing leg also termed as a push off at the end of single support, followed by an eccentric flexion of the leading leg performing majority of power absorption within the double support phase [9,25,26].

There have been attempts to replace the dissipated energy during contact with force impulses to the stance leg just before heel strike [2,9]. However assuming infinitesimal impulse time duration is not practical for real mechanisms. Miossec and Aoustin [14] presented a model that included finite time duration of double support in a gait cycle but without preceding push off. The advantage of push off was shown in [18], where the adaptive implicit push off control as part of feedback control in biped model with telescopic legs significantly contributed to settling in stable state space orbit with desired gait velocity.

This paper extends the two-level control strategy as applied in a model with telescopic legs [18] to allow adaptive control of a human-like biped walking model with ankles, knees, pelvis and torso. The notion of virtual leg is introduced and corresponding control strategy developed to enable versatility in a set of gait patterns. Resulting gait patterns will be assessed in relation to particular aspect of human locomotion.

2. Robot model and modeling assumption

The biped walking model is considered planar with eight degrees of freedom. Thigh, shank and foot segments are connected at knee and ankle by ideal revolute joint to form each leg. Both legs are connected at hip joint by ideal revolute joint and carry pelvis and torso segments, both linked by ideal revolute joint. There is a point mass at the center of each segment and additional mass at the hip joint. Each joint is actuated via torque actuator with the rotational axis aligned with joint axis. A representative model structure is shown in Fig. 1 and model parameters are gathered in Table 1.

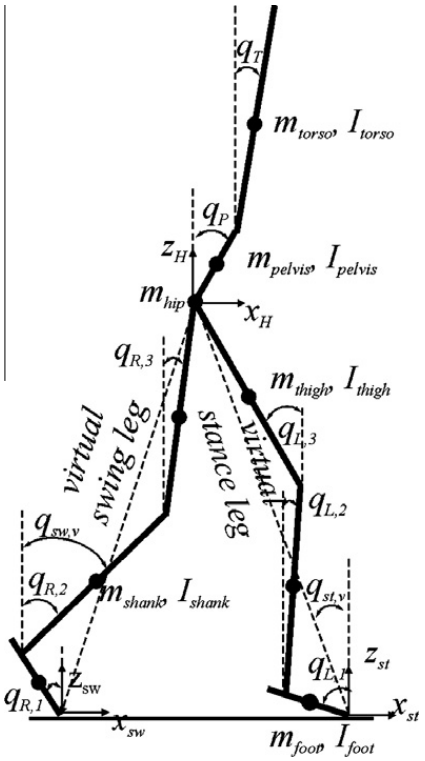

Fig. 1. Schematic representation of the biped walking model.

Author's personal copy

Table 1
Model parameters.

Segment	Mass (kg)	Length (m)	Inertia (kg m^2)
Foot	1	0.15	0.2
Shank	5	0.5	0.6
Thigh	7	0.5	0.8
Hip	10	–	–
Pelvis	7	0.15	0.8
Torso	35	0.4	3.0

Complete gait cycle is divided into phases of single support (associated with the stance leg touching the ground and the swing leg advancing towards the point of new contact) and double support (associated with the stance as well as swing leg touching the ground and the legs are referred to according to their function in the preceding single support phase). Transition from single support to double support phase is contact phase and is associated with the swing leg touching the ground. Similarly, the transition from double support to single support phase is referred to as the take-off phase and is associated with the rear leg lifting of the ground. Both transition phases are assumed to be instantaneous. Additionally, when either left or right leg is in contact with the ground only toe contact will be assumed, whereas keeping the heel above the ground is assured by corresponding control assumption provided in later section. The dynamic equations are composed of ordinary differential equations for the support phases and algebraic equations for the transition phases.

2.1. Single support phase

Let $\boldsymbol{q} = (q_{L,1}, q_{L,2}, q_{L,3}, q_{R,1}, q_{R,2}, q_{R,3}, q_P, q_T, x_H, z_H)^T$ be the set of coordinates describing the configuration of the robot with respect to world reference frame and let $\boldsymbol{u} = (T_{L,1}, T_{L,2}, T_{L,3}, T_{R,1}, T_{R,2}, T_{R,3}, T_T)^T$ be the joint torques associated with corresponding joint axes. To account for switching between the single and double support phases we further denote $q_{1,st} = q_{L,1}$, $q_{2,st} = q_{L,2}$, $q_{3,st} = q_{L,3}$, $q_{1,sw} = q_{R,1}$, $q_{2,sw} = q_{R,2}$, $q_{3,sw} = q_{R,3}$ and $T_{1,st} = T_{L,1}$, $T_{2,st} = T_{L,2}$, $T_{3,st} = T_{L,3}$, $T_{1,sw} = T_{R,1}$, $T_{2,sw} = T_{R,2}$, $T_{3,sw} = T_{R,3}$ when left and right legs are considered as stance and swing leg respectively in a current single support and succeeding double support phase. Likewise we will denote $q_{1,st} = q_{R,1}$, $q_{2,st} = q_{R,2}$, $q_{3,st} = q_{R,3}$, $q_{1,sw} = q_{L,1}$, $q_{2,sw} = q_{L,2}$, $q_{3,sw} = q_{L,3}$ and $T_{1,st} = T_{R,1}$, $T_{2,st} = T_{R,2}$, $T_{3,st} = T_{R,3}$, $T_{1,sw} = T_{L,1}$, $T_{2,sw} = T_{L,2}$, $T_{3,sw} = T_{L,3}$ when right and left legs are considered as swing and stance leg respectively in current single support and succeeding double support phase.

Two constraint equations $x_{st} = const$, $z_{st} = 0$ account for the stance leg contacting the ground throughout the single support phase. They reduce the feasible space of motion to a constraint surface and when organized in matrix form $\boldsymbol{\Psi}_{ss}(\boldsymbol{q}) = \boldsymbol{0}$ they can be introduced into dynamic Euler-Lagrange equations of constrained system through Lagrange multipliers:

$$\begin{aligned} &\boldsymbol{M}(\boldsymbol{q})\ddot{\boldsymbol{q}} + \boldsymbol{C}(\boldsymbol{q},\dot{\boldsymbol{q}})\dot{\boldsymbol{q}} + \boldsymbol{G}(\boldsymbol{q}) = \boldsymbol{B}\boldsymbol{u} + \boldsymbol{\Gamma}_{ss}^T\boldsymbol{\lambda}_{ss} \\ &\boldsymbol{\Gamma}_{ss}\dot{\boldsymbol{q}} = \frac{\partial \boldsymbol{\Psi}_{ss}}{\partial \boldsymbol{q}}\dot{\boldsymbol{q}} = \boldsymbol{0} \end{aligned} \qquad T_{ss,start} < t < T_{ss,end} \tag{1}$$

where $\boldsymbol{M}(\boldsymbol{q})$ is the inertia matrix, $\boldsymbol{C}(\boldsymbol{q},\dot{\boldsymbol{q}})$ is the matrix of centripetal and Coriolis terms, $\boldsymbol{G}(\boldsymbol{q})$ is the gravity vector and $\boldsymbol{\lambda}_{ss}$ is a vector of Lagrange multipliers equal to negative ground reaction forces during single support. $T_{ss,start}$ and $T_{ss,end}$ denote the times of the start and the end of single support phase respectively. The model is written in the state space form by:

$$\dot{\boldsymbol{x}}_{ss} = \begin{bmatrix} \dot{\boldsymbol{q}} \\ \boldsymbol{M}^{-1}(\boldsymbol{q})\left[-\boldsymbol{C}(\boldsymbol{q},\dot{\boldsymbol{q}})\dot{\boldsymbol{q}} - \boldsymbol{G}(\boldsymbol{q}) + \boldsymbol{B}\boldsymbol{u} + \boldsymbol{\Gamma}_{ss}^T\boldsymbol{\lambda}_{ss}\right] \end{bmatrix} =: \boldsymbol{f}_{ss}(\boldsymbol{x}_{ss}) + \boldsymbol{g}_{ss}(\boldsymbol{x}_{ss})\boldsymbol{u} \tag{2}$$

2.2. Contact phase

A standard rigid contact model is assumed [7]. The impact is considered instantaneous and without slipping. Furthermore, the external forces during the impact can be represented by impulses and cannot be generated by actuators, whereas the impulse forces may result in velocity but not position discontinuities. This implies the conservation of angular momentum:

$$\boldsymbol{M}(\dot{\boldsymbol{q}}^+ - \dot{\boldsymbol{q}}^-) = \boldsymbol{F}_{c,ext} \tag{3}$$

In (3) $\dot{\boldsymbol{q}}^+$ and $\dot{\boldsymbol{q}}^-$ are velocity vectors just after and just before the impact respectively and $\boldsymbol{F}_{c,ext}$ the contact impulse forces.

Four constraint equations in the form $x_{st} = const_1$, $z_{st} = 0$, $x_{sw} = const_2$ and $z_{sw} = 0$ completely characterize the contacts of both legs with the ground after the impact and are organized in matrix form $\boldsymbol{\Psi}_c(\boldsymbol{q}) = \boldsymbol{0}$. The following relation determines the admissible set of velocities after the impact:

$$\boldsymbol{\Gamma}_c\dot{\boldsymbol{q}}^+ = \frac{\partial \boldsymbol{\Psi}_c}{\partial \boldsymbol{q}}\dot{\boldsymbol{q}}^+ = \boldsymbol{0} \tag{4}$$

Author's personal copy

With additional equation relating the impulse during contact $\boldsymbol{F_{c,ext}}$ to the tangent and normal forces during contact $\boldsymbol{F_c}$ at the tips of both legs

$$\boldsymbol{F}_{c,ext} = \boldsymbol{\Gamma}_c^T(\boldsymbol{q}_c)[\,F_{T1} \quad F_{N1} \quad F_{T2} \quad F_{N2}\,]^T = \boldsymbol{\Gamma}_c^T(\boldsymbol{q}_c)\boldsymbol{F}_c \tag{5}$$

the following set of equations is solved for joint velocities just after the impact $\dot{q}^+$

$$\begin{bmatrix} \boldsymbol{M} & -\boldsymbol{\Gamma}_c^T \\ \boldsymbol{\Gamma}_c & \boldsymbol{0} \end{bmatrix} \cdot \begin{bmatrix} \dot{\boldsymbol{q}}^+ \\ \boldsymbol{F}_c \end{bmatrix} = \begin{bmatrix} \boldsymbol{M}\dot{\boldsymbol{q}}^- \\ \boldsymbol{0} \end{bmatrix} \quad t = T_c = T_{ss,end} = T_{ds,start} \tag{6}$$

where T_c denotes the contact time and (6) illustrates instantaneous transition to double support. Geometrically the contact model can also be considered as an $\boldsymbol{M}(\boldsymbol{q})$ – orthogonal projections of $\dot{\boldsymbol{q}}^-$ onto the feasible space $\{\dot{\boldsymbol{q}}^+ \in \boldsymbol{T}_q\boldsymbol{Q} | \boldsymbol{\Gamma}_c\dot{\boldsymbol{q}}^+ = \boldsymbol{0}\}$ [21].

2.3. Double support phase

Four constraint equations $x_{st} = const_1$, $z_{st} = 0$, $x_{sw} = const_2$, $z_{sw} = 0$ account for both legs contacting the ground throughout the single support phase. They reduce the feasible space of motion to a constraint surface and when organized in matrix form $\boldsymbol{\Psi}_{ss}(\boldsymbol{q}) = \boldsymbol{0}$ they can be introduced into dynamic Euler-Lagrange equations of constrained system through Lagrange multipliers:

$$\begin{aligned} &\boldsymbol{M}(\boldsymbol{q})\ddot{\boldsymbol{q}} + \boldsymbol{C}(\boldsymbol{q},\dot{\boldsymbol{q}})\dot{\boldsymbol{q}} + \boldsymbol{G}(\boldsymbol{q}) = \boldsymbol{B}\boldsymbol{u} + \boldsymbol{\Gamma}_{ds}^T\boldsymbol{\lambda}_{ds} \\ &\boldsymbol{\Gamma}_{ds}\dot{\boldsymbol{q}} = \frac{\partial \boldsymbol{\Psi}_{ds}}{\partial \boldsymbol{q}}\dot{\boldsymbol{q}} = \boldsymbol{0} \end{aligned} \qquad T_{ds,start} < t < T_{ds,end} \tag{7}$$

where $\boldsymbol{\lambda}_{ds}$ is a vector of Lagrange multipliers equal to negative ground reaction forces during double support. $T_{ds,start}$ and $T_{ds,end}$ denote the times of the start and end of double support phase respectively. The model is written in the state space form:

$$\dot{\boldsymbol{x}}_{ds} = \begin{bmatrix} \dot{\boldsymbol{q}} \\ \boldsymbol{M}^{-1}(\boldsymbol{q})\left[-\boldsymbol{C}(\boldsymbol{q},\dot{\boldsymbol{q}})\dot{\boldsymbol{q}} - \boldsymbol{G}(\boldsymbol{q}) + \boldsymbol{B}\boldsymbol{u} + \boldsymbol{\Gamma}_{ds}^T\boldsymbol{\lambda}_{ds}\right] \end{bmatrix} =: \boldsymbol{f}_{ds}(\boldsymbol{x}_{ds}) + \boldsymbol{g}_{ds}(\boldsymbol{x}_{ds})\boldsymbol{u} \tag{8}$$

2.4. Take-off phase

Take-off phase is transition phase between double support phase and succeeding single support phase. Considering that only one leg remains in contact with the ground in succeeding single support phase, the take-off phase transition model has to account for two constraint equations in the form $x_{st} = const$, $y_{st} = 0$ or organized in matrix form $\boldsymbol{\Psi}_{top}(\boldsymbol{q}) = \boldsymbol{0}$. Hence, by adjusting the transition model of the contact phase in this sense the transition model of the contact phase can be rewritten to obtain the transition model of the take-off phase, thus expressing the relation between velocities just before and just after the take-off:

$$\begin{bmatrix} \boldsymbol{M} & -\boldsymbol{\Gamma}_{top}^T \\ \boldsymbol{\Gamma}_{top} & \boldsymbol{0} \end{bmatrix} \cdot \begin{bmatrix} \dot{\boldsymbol{q}}^+ \\ \boldsymbol{F}_{top} \end{bmatrix} = \begin{bmatrix} \boldsymbol{M}\dot{\boldsymbol{q}}^- \\ \boldsymbol{0} \end{bmatrix} \quad t = T_{top} = T_{ds,end} = T_{ss,start} \tag{9}$$

where $\boldsymbol{\Gamma}_{top} = \frac{\partial \boldsymbol{\Psi}_{top}}{\partial \boldsymbol{ds}}$, $\dot{\boldsymbol{q}}^+$ and $\dot{\boldsymbol{q}}^-$ are velocities just after and just before the take-off respectively, $\boldsymbol{F}_{top}$ represents tangent and normal forces at the tip of the leg, that remains in contact with the ground in succeeding single support phase, $\boldsymbol{T_{top}}$ denotes the contact time. Geometrically the transition model of the take-off phase can also be considered as an $\boldsymbol{M}(\boldsymbol{q})$ – orthogonal projections of $\dot{\boldsymbol{q}}^-$ onto the feasible space $\{\dot{\boldsymbol{q}}^+ \in \boldsymbol{T}_q\boldsymbol{Q} | \boldsymbol{\Gamma}_{top}\dot{\boldsymbol{q}}^+ = \boldsymbol{0}\}$ [21].

3. Control strategy

The following section extends the two-level control strategy as described in [18] to apply for a model with knees and ankles as well as pelvis segment. The lower within-step control level adopts trajectory tracking via feedback control, where the walking mechanisms are encoded in postural terms that are expressed as a set of holonomic constraints of the kinematic variables and as outputs of the model imposed on the robot via feedback control. These constraints are adaptively modified after each gait cycle on higher, between-step control level in such a manner to adjust forward propulsion to achieve desired gait velocity and step length.

3.1. Within-step control

3.1.1. Within-step control in single support phase

Human walking is characterized with roughly symmetrical movement of the stance and swing leg, sufficient foot clearance for the swing leg to advance towards the point of new contact, small sways in nearly vertical torso as well as pelvis positions and minimal vertical hip movement. These general observations form the following set of control objectives:

Author's personal copy

$$\begin{aligned} y_1 &= q_{st,v} + q_{sw,v} - r_1 \\ y_2 &= z_{sw} - r_2 \\ y_3 &= q_T - r_3 \\ y_4 &= q_P - r_4 \\ y_5 &= L_{st,v} - r_5 \end{aligned} \tag{10}$$

where $L_{st,v}$ is the virtual stance leg length

$$L_{st,v} = |\boldsymbol{p}_H - \boldsymbol{p}_{st}| \tag{11}$$

and r_i, $i = 1, \ldots, 5$ are reference trajectories to be followed

$$\begin{aligned} r_1 &= (q_{st,v} + q_{sw,v})|_{t=T_{ss,start}} \times w_{ss,1} \\ r_2 &= \tfrac{L_{leg,nominal}}{k_1} \times (q_{st,v,d} \times w_{ss,2} + q_{st,v}|_{t=T_{ss,start}} \times w_{ss,3} - q_{st,v}) \\ r_3 &= q_T|_{t=T_{ss,start}} \times w_{ss,4} + q_{T,d} \times w_{ss,5} \\ r_4 &= q_{P,d}(q_{st,v}) \\ r_5 &= L_{st,v,d}(q_{st,v}) \end{aligned} \tag{12}$$

Tracing the reference trajectory r_1 implies symmetrical gait of the biped walking model, with exponential pattern assured by an appropriately selected exponential function $w_{ss,1}$ with time constant sufficiently smaller than the time duration of single support phase. Such definition sets $q_{st,v}$ to be a monotonically increasing function during single support phase $q_{st,v} \in \left[q_{st,v}|_{t=T_{ss,start}}, q_{st,v}|_{t=T_{ss,end}}\right]$. Likewise, the reference trajectory r_2 ensures the swing leg to avoid colliding with the ground while progressing. It is assumed that when $q_{st,v}|_{t=T_{ss,end}} = q_{st,v,d}$, the tip of the swing leg touches the ground and the single support phase terminates. $q_{st,v,d}$ is a desired virtual stance leg angle at the end of single support phase and is related to desired gait velocity $v_{gait,d}$, desired cadence $cad_{gait,d}$ and desired step length $L_{step,d}$ by

$$L_{step,d} = \frac{2v_{gait,d}}{cad_{gait,d}} = x_{st}|_{t=T_{ss,start}} - x_{sw}|_{t=T_{ss,start}} + 2L_{leg,nominal}\sin(q_{st,v,d}) \tag{13}$$

Reference trajectory r_2 sets the foot clearance to be proportional to nominal length of the virtual stance leg $L_{st,nominal}$. $w_{ss,2}$ and $w_{ss,3}$ are exponential functions with time constant sufficiently smaller than the time duration of single support phase that assures smooth exponential pattern.

Zeroing the output function y_3 via feedback control ensures the biped walking model is tracing the reference trajectory r_3, thus maintaining the torso segment at the desired angle with respect to the vertical. To assure smooth exponential transition from initial torso angle at the start of the single support phase towards desired torso angle $q_{T,d}$, $w_{ss,4}$ and $w_{ss,5}$ exponential functions with time constant sufficiently smaller than the time duration of single support were chosen. Similarly, pelvis segment exhibits small sways in sagittal plane as determined by the reference trajectory r_4. It is defined as a fifth-order polynomial of virtual stance leg angle $q_{st,v}$ such that (see Fig. 2 for representation)

$$\begin{aligned} &q_P(q_{st,v}|_{t=T_{ss,start}}) = q_P|_{t=T_{ss,start}} \\ &q_P\left(q_{st,v} = \tfrac{q_{st,v}|_{t=T_{ss,start}} + q_{st,v,d}}{2}\right) = k_2 \times q_{P,nominal} \\ &q_P(q_{st,v,d}) = q_{P,nominal} \\ &\dot{q}_P\left(q_{st,v} = \tfrac{q_{st,v}|_{t=T_{ss,start}} + q_{st,v,d}}{2}\right) = 0 \\ &\dot{q}_P(q_{st,v}|_{t=T_{ss,start}}) = \dot{q}_{P,d}|_{t=T_{ss,start}} \\ &\dot{q}_P(q_{st,v,d}) = \dot{q}_{P,d}|_{t=T_{ss,end}} \end{aligned} \tag{14}$$

where $q_{P,nominal}$ is a desired pelvic midpoint sway and k_2 is a coefficient to determine the pelvic midsway magnitude.

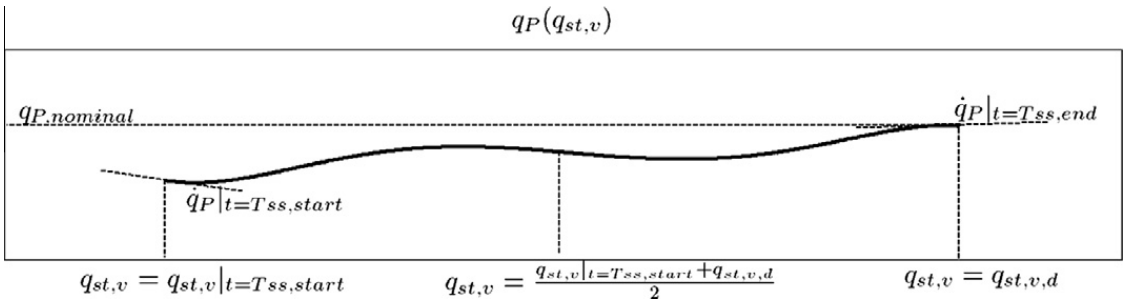

Fig. 2. Fifth-order polynomial representing reference trajectory $r_4 = q_P(q_{st,v})$.

Author's personal copy

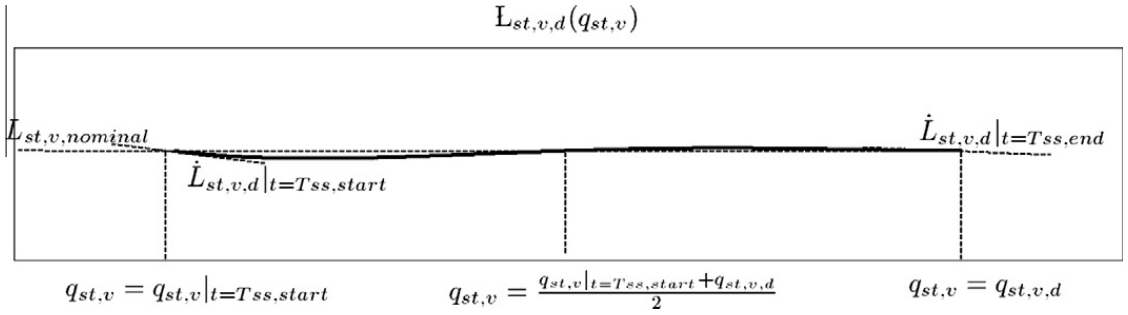

Fig. 3. Forth-order polynomial representing reference trajectory $r_5 = L_{st,v,d}(q_{st,v})$.

Lengthening and shortening of virtual stance leg as defined by reference trajectory r_5 determines the movement of the stance leg. It is defined as a forth-order polynomial of $q_{st,v}$ such that (Fig. 3):

$$\begin{aligned}
&L_{st,v}(q_{st,v}|_{t=T_{ss,start}}) = L_{st,v}|_{t=T_{ss,start}}\\
&L_{st,v}\left(q_{st,v} = \frac{q_{st,v}|_{t=T_{ss,start}}+q_{st,v,d}}{2}\right) = L_{st,v,nominal}\\
&L_{st,v}(q_{st,v,d}) = L_{st,nominal}\\
&\dot{L}_{st,v}(q_{st,v}|_{t=T_{ss,start}}) = \dot{L}_{st,v}|_{t=T_{ss,start}}\\
&\dot{L}_{st,v}(q_{st,v,d}) = \dot{L}_{st,v,d}|_{t=T_{ss,end}}
\end{aligned} \tag{15}$$

where $\dot{L}_{st,v,d}|_{t=T_{ss,end}}$ is desired virtual stance leg lengthening velocity at the end of single support phase which is determined on between-step control level to assure adaptive push off control and hence desired gait velocity control.

Although relations y_i, $i = 1, \ldots, 5$ sufficiently describe stable gait for a biped walking model, two additional relations are needed to assure full rank of (2) and to calculate two remaining joint moments. They can be determined to emphasize certain walking aspects that can be observed in human walking as well. Although in described biped walking model a virtual stance leg lengthening control will assure sufficient propulsion for the model to settle in stable gait, the present control scheme does not provide any insight about the source of propulsion. In human gait the majority of propulsion comes from rapid ankle joint extension at the end of single support phase. Similar process can be implemented in presented biped walking model by enforcing the desired lengthening and/or shortening of virtual stance leg ankle component (Fig. 4) via feedback control. Two additional output functions can be formed as follows:

$$\begin{aligned}
y_6 &= L_{st,ankle,v} - r_6\\
y_7 &= L_{sw,ankle,v} - r_7
\end{aligned} \tag{16}$$

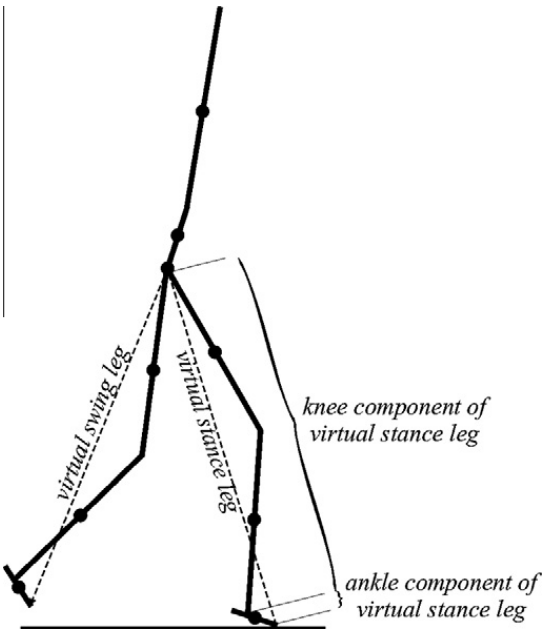

Fig. 4. Ankle and knee components of virtual stance leg.

Author's personal copy

where $L_{st,ankle,v}$ is the length of the virtual stance leg ankle component

$$L_{st,ankle,v} = (\boldsymbol{p}_{st,ankle} - \boldsymbol{p}_{st}) \cdot \frac{(\boldsymbol{p}_H - \boldsymbol{p}_{st})^T}{|\boldsymbol{p}_H - \boldsymbol{p}_{st}|} \tag{17}$$

$L_{sw,ankle,v}$ is the length of the virtual swing leg ankle component

$$L_{sw,ankle,v} = (\boldsymbol{p}_{sw,ankle} - \boldsymbol{p}_{sw}) \cdot \frac{(\boldsymbol{p}_H - \boldsymbol{p}_{sw})^T}{|\boldsymbol{p}_H - \boldsymbol{p}_{sw}|} \tag{18}$$

and r_6, r_7 are reference trajectories to be followed

$$\begin{aligned} r_6 &= L_{st,ankle,v,d}(q_{st,v}) \\ r_7 &= L_{sw,ankle,v,d}(q_{st,v}) \end{aligned} \tag{19}$$

Additionally, in (17) and (18) $\boldsymbol{p_{st,ankle}}$ and $\boldsymbol{p_{sw,ankle}}$ denote positions of the stance leg ankle joint and swing leg ankle joint respectively.

Reference trajectory r_6 is a forth-order polynomial (Fig. 5) determined by:

$$\begin{aligned} &L_{st,ankle,v}(q_{st,v}|_{t=T_{ss,start}}) = L_{st,ankle,v}|_{t=T_{ss,start}} \\ &L_{st,ankle,v}\left(q_{st,v} = \tfrac{q_{st,v}|_{t=T_{ss,start}} + q_{st,v,d}}{2}\right) = k_M \cdot L_{st,ankle,v}|_{t=0} \\ &L_{st,ankle,v}(q_{st,v}|_{t=T_{ss,end}}) = k_E \cdot L_{st,ankle,v}|_{t=0} \\ &\dot{L}_{st,ankle,v}(q_{st,v}|_{t=T_{ss,start}}) = \dot{L}_{st,ankle,v}|_{t=T_{ss,start}} \\ &\dot{L}_{st,ankle,v}(q_{st,v}|_{t=T_{ss,end}}) = \dot{L}_{st,ankle,v,d} \end{aligned} \tag{20}$$

In (20) $\dot{L}_{st,ankle,v,d}$ denotes a desired lengthening velocity of ankle component at the end of single support phase and k_M and k_E are constants that determine the length amplitudes of virtual stance leg ankle component at midstance phase and the end of the stance phase respectively. k_M and k_E values were selected in a way to assure $L_{st,ankle,v}$ is large enough so that the heel is always above the toe and cannot touch the ground. Note that by arbitrarily setting $\dot{L}_{st,ankle,v,d}$ we can establish a desired propulsion distribution between ankle and knee joints, hence generating various gait patterns.

The length dynamics of the virtual swing leg ankle component has considerably less impact on overall gait dynamics of the model. For these reason the motion of the swing leg ankle component is determined by a simple linear regression from initial value at the start of swing phase to end value, which is the same as of the virtual stance leg ankle component at the start of the simulation.

Complete output vector in single support phase reads as

$$\boldsymbol{y}_{ss} = \boldsymbol{h}_{ss}(\boldsymbol{q}) = \begin{bmatrix} q_{st,v} + q_{sw,v} - r_1 \\ z_{sw} - r_2 \\ q_T - r_3 \\ q_P - r_4 \\ L_{st,v} - r_5 \\ L_{st,ankle,v} - r_6 \\ L_{sw,ankle,v} - r_7 \end{bmatrix} \tag{21}$$

3.1.2. Within-step control in double support phase

In double support phase a weight transfers onto the opposite leg. Since there are four constraints in double support phase that describe the contacts of both legs with the ground, we can choose only six linearly independent output functions to

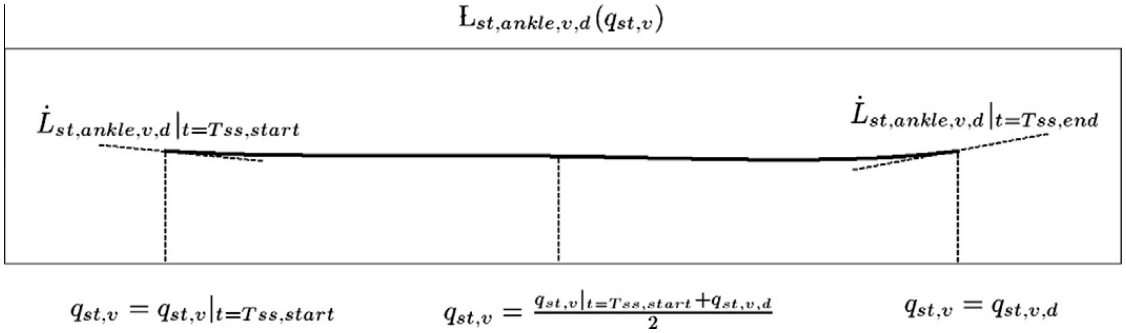

Fig. 5. Forth-order polynomial representing reference trajectory $r_6 = L_{st,ankle,v,d}(q_{st,v})$.

Author's personal copy

describe the motion of the model. Compared to single support phase double support phase is a considerably shorter phase with smaller range of joint motion and only small discrepancies in walking characteristics. Enforcing symmetry in double support phase would prevent proper weight transfer onto the opposite leg, which is inconsistent with general forward progression of body center. Similarly, since both legs are in contact with the ground, foot clearance should be suspended from the walking premises. This yields the following modified set of output functions in double support:

$$\begin{aligned} y_1 &= q_{st,v} + q_{sw,v} - r_1 \\ y_2 &= q_T - r_2 \\ y_3 &= q_P - r_3 \\ y_4 &= L_{st,v} - r_4 \\ y_5 &= L_{st,ankle,v} - r_5 \\ y_6 &= L_{sw,ankle,v} - r_6 \end{aligned} \tag{22}$$

In (22) r_i, $i = 1, \ldots, 6$ represent the reference trajectories to be followed in double support. Since the range of motion is small in double support, the choice of reference trajectories is considerably simplified. They were defined as slow functions with convergence assured by exponential functions with small time constant $w_{ds,1}$, $w_{ds,2}$, $w_{ds,3}$, $w_{ds,4}$, $w_{ds,5}$, $w_{ds,6}$

$$\begin{aligned} r_1 &= (q_{st,v} + q_{sw,v})|_{t=Tds,start} \times w_{ds,1} \\ r_2 &= q_T|_{t=Tds,start} \times w_{ds,2} \\ r_3 &= q_P|_{t=Tds,start} \times w_{ds,3} \\ r_4 &= L_{st,v}|_{t=Tds,start} \times w_{ds,4} \\ r_5 &= L_{st,ankle,v}|_{t=Tds,start} \times w_{ds,5} \\ r_6 &= L_{sw,ankle,v}|_{t=Tds,start} \times w_{ds,6} \end{aligned} \tag{23}$$

The output vector in double support phase reads as

$$\boldsymbol{y}_{ds} = \boldsymbol{h}_{ds}(\boldsymbol{q}) = \begin{bmatrix} q_{st,v} + q_{sw,v} - r_1 \\ q_T - r_2 \\ q_P - r_3 \\ L_{st,v} - r_4 \\ L_{st,ankle,v} - r_5 \\ L_{sw,ankle,v} - r_6 \end{bmatrix} \tag{24}$$

3.1.3. Controller design

Control objective is to drive the output vectors in single support phase $\boldsymbol{y}_{ss} = \boldsymbol{h}_{ss}(\boldsymbol{q})$ as well as in double support phase $\boldsymbol{y}_{ds} = \boldsymbol{h}_{ds}(\boldsymbol{q})$ to zero. Since both depend only on configuration variables, the relative degree of output vectors is two. By following the standard Lie derivative notation [8], the second derivation yields

$$\begin{aligned} \ddot{\boldsymbol{y}}_{ss} &= \boldsymbol{L}_{f_{ss}}^{\boldsymbol{2}} \boldsymbol{h}_{ss}(\boldsymbol{q}, \dot{\boldsymbol{q}}) + \boldsymbol{L}_{g_{ss}} \boldsymbol{L}_{f_{ss}} \boldsymbol{h}_{ss}(\boldsymbol{q}) \boldsymbol{u}_{ss} \\ \ddot{\boldsymbol{y}}_{ds} &= \boldsymbol{L}_{f_{ds}}^{\boldsymbol{2}} \boldsymbol{h}_{ds}(\boldsymbol{q}, \dot{\boldsymbol{q}}) + \boldsymbol{L}_{g_{ds}} \boldsymbol{L}_{f_{ds}} \boldsymbol{h}_{ds}(\boldsymbol{q}) \boldsymbol{u}_{ds} \end{aligned} \tag{25}$$

Therefore, in single support phase the applied feedback is given by

$$\boldsymbol{u}_{ss} = -(\boldsymbol{L}_{g_{ss}} \boldsymbol{L}_{f_{ss}} \boldsymbol{h}_{ss})^{-1} \left(\boldsymbol{L}_{f_{ss}}^{\boldsymbol{2}} \boldsymbol{h}_{ss} + \boldsymbol{K}_{D,ss} \boldsymbol{L}_{f_{ss}} \boldsymbol{h}_{ss} + \boldsymbol{K}_{P,ss} \boldsymbol{h}_{ss} \right) \tag{26}$$

where $\boldsymbol{L}_g \boldsymbol{L}_f \boldsymbol{h}(q)$ is the decoupling matrix and is assumed invertible and $\boldsymbol{K}_D$ and $\boldsymbol{K}_P$ are positive definite gain matrices.

On the other hand, since in double support phase there are only six reference trajectories available to determine seven unknown motor actuations, $\boldsymbol{L}_g \boldsymbol{L}_f \boldsymbol{h}(q)$ in double support is no longer invertible and the solution is not unique. For this reason, to determine the unknown motor actuations in double support, we used standard Moore–Penrose pseudoinverse:

$$\boldsymbol{u}_{ds} = -(\boldsymbol{L}_{g_{ds}} \boldsymbol{L}_{f_{ds}} \boldsymbol{h}_{ds})^{+} \left(\boldsymbol{L}_{f_{ds}}^{\boldsymbol{2}} \boldsymbol{h}_{ds} + \boldsymbol{K}_{D,ds} \boldsymbol{L}_{f_{ds}} \boldsymbol{h}_{ds} + \boldsymbol{K}_{P,ds} \boldsymbol{h}_{ds} \right) \tag{27}$$

where the superscript $^+$ denotes

$$A^{+} = (A^T A)^{-1} A^T \tag{28}$$

Internal dynamics of the system when the outputs $\boldsymbol{y}_{ss}(\boldsymbol{q})$ and $\boldsymbol{y}_{ds}(\boldsymbol{q})$ are identically zero is referred to as zero dynamics. Thus,

$$\begin{aligned} \boldsymbol{Z}_{ss} &= \{(\boldsymbol{q}', \dot{\boldsymbol{q}}') \in \boldsymbol{TQ} | \boldsymbol{h}_{ss}(\boldsymbol{q}) = 0, \boldsymbol{L}_f \boldsymbol{h}_{ss}(\boldsymbol{q}) = \boldsymbol{0}\} \\ \boldsymbol{Z}_{ds} &= \{(\boldsymbol{q}', \dot{\boldsymbol{q}}') \in \boldsymbol{TQ} | \boldsymbol{h}_{ds}(\boldsymbol{q}) = \boldsymbol{0}, \boldsymbol{L}_f \boldsymbol{h}_{ds}(\boldsymbol{q}) = \boldsymbol{0}\} \end{aligned} \tag{29}$$

denote zero dynamics of single and double support respectively.

Author's personal copy

3.2. Between-step control

Prior to next single support phase between-step control adaptively varies the desired stance leg lengthening velocity at the end of single support phase $\dot{L}_{st,d}|_{t=T_{ss,end}}$ according to gait velocity deviation from the desired gait velocity. It acts in a sense that greater $\dot{L}_{st,d}|_{t=T_{ss,end}}$ implies more pronounced push off, i.e. forward propulsion, which eventually results in faster gait velocity and vice versa. Between-step control algorithm can be expressed as

$$\dot{L}^{k}_{st,d}\Big|_{t=T_{ss,end}} = \dot{L}^{k-1}_{st,d}|_{t=T_{ss,end}} + k_p\left(v^{k-1}_{gait} - v_{gait,d}\right) + k_d\left(v^{k-1}_{gait} - v^{k-2}_{gait}\right) \tag{30}$$

where the superscript k indicates the gait cycle number, k_d and k_p are positive gains and

$$v^{k}_{gait} = \frac{x^{k}_{H}\big|_{t=T_{ds,end}} - x^{k}_{H}\big|_{t=T_{ss,start}}}{T_{ds,end} - T_{ss,start}} \tag{31}$$

Such definition of $\dot{L}_{st,d}|_{t=T_{ss,end}}$ control directly indicates an adaptive nature of single support output vector $\boldsymbol{h}_{ss}(\boldsymbol{q})$, which further implies time-variability of single support zero dynamics

$$\boldsymbol{Z}_{ss} = \boldsymbol{Z}_{ss}(\boldsymbol{k}) = \{(\boldsymbol{q}', \dot{\boldsymbol{q}}') \in \boldsymbol{TQ} | \boldsymbol{h}_{ss}(\boldsymbol{q}, k) = \boldsymbol{0}, \boldsymbol{L}_f \boldsymbol{h}_{ss}(\boldsymbol{q}, k) = \boldsymbol{0}\} \tag{32}$$

Complete control strategy is illustrated in Fig. 6.

4. Simulation cases

Three sets of simulation cases (Table 2) were selected to test the performance of the proposed adaptive control strategy in a wide range of walking modes and to relate the deviations between gait patterns due to parameter variation to human locomotion mechanisms in terms of power absorption and push off: (i) in first set of simulation cases (Case 1–3) we investigated the effect of increasing gait velocity; extensive biomechanical studies show that in human locomotion greater gait velocity is accompanied with more pronounced power absorption and push off. (ii) Second set of simulation cases (Case 2, Case 4–5) addressed torso angle variations; in human locomotion one observes that anteriorly inclined torso shifts the center of mass forward, which contributes significantly to downward fall, thus exhibiting more pronounced power absorption and less dis-

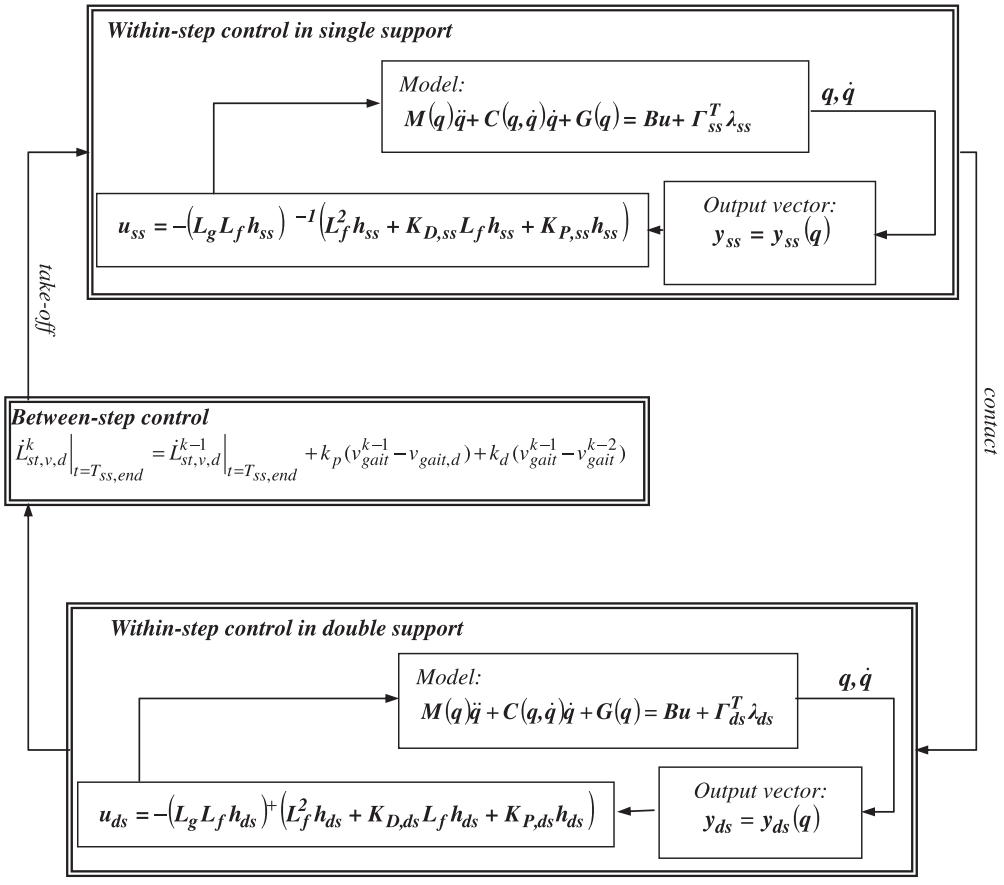

Fig. 6. Schematic representation of the complete control strategy.

Author's personal copy

Table 2
Simulation cases: desired kinematics parameters.

	Case 1	Case 2	Case 3	Case 4	Case 5	Case 6	Case 7
$v_{gait,d}$ (m/s)	0.8	0.9	1	0.9	0.9	0.9	0.9
$q_{T,d}$ (rad)	0	0	0	0.1	0.2	0	0
$cad_{gait,d}$ (steps/min)	110	110	110	110	110	110	110
$\dot{L}_{st,ankle,v,d}$ (m/s)	0.2	0.2	0.2	0.2	0.2	0.1	0.3

tinctive push off. (iii) Third set of simulation cases (Case 2, Case 6–7) focused on different propulsion distribution profiles $\dot{L}_{st,ankle,v,d}$ between knee and ankle joints; such walking mode exhibits a typical pathological gait mechanism, where the inability to perform satisfactory in one joint forces dominant engagement of the other joint.

$\boldsymbol{K}_{D,ss}$, $\boldsymbol{K}_{P,ss}$, $\boldsymbol{K}_{D,ds}$, $\boldsymbol{K}_{D,ds}$, k_p and k_d were determined on the basis of test simulations prior to simulation start and remained unchanged in all simulation cases.

5. Results

Fig. 7 displays a set of state space orbits for each simulation case. Cyclic behavior of each state space orbit in all simulation cases implies that the proposed adaptive control strategy induces a stable walking for a biped walking model in a wide range of walking modes. A demonstrative performance of the proposed adaptive control strategy in simulation case Case 3 is

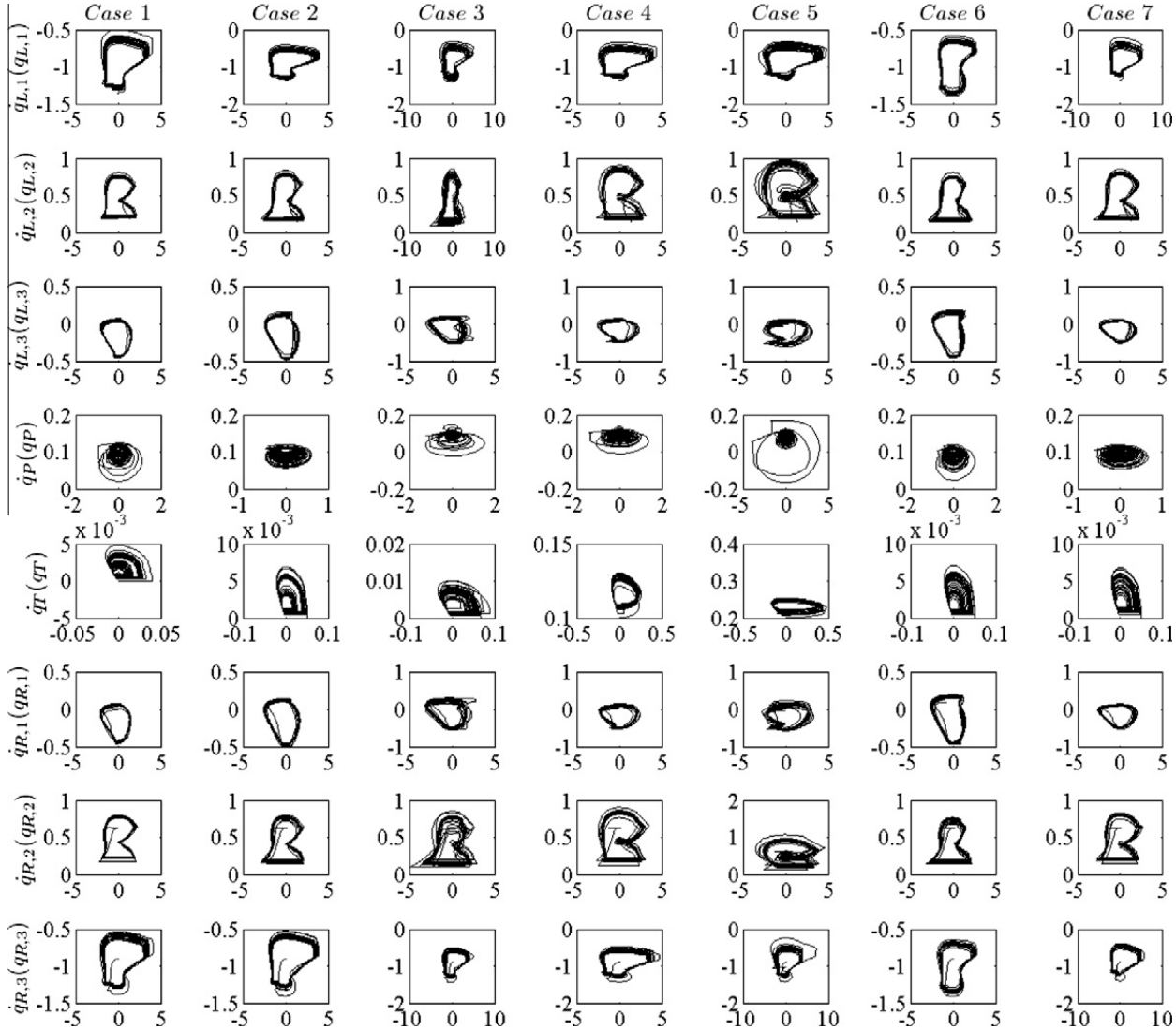

Fig. 7. State space orbits for all simulation cases. Each orbit is parameterized with respect to configuration variable (horizontal axis) and its derivative (vertical axis).

Author's personal copy

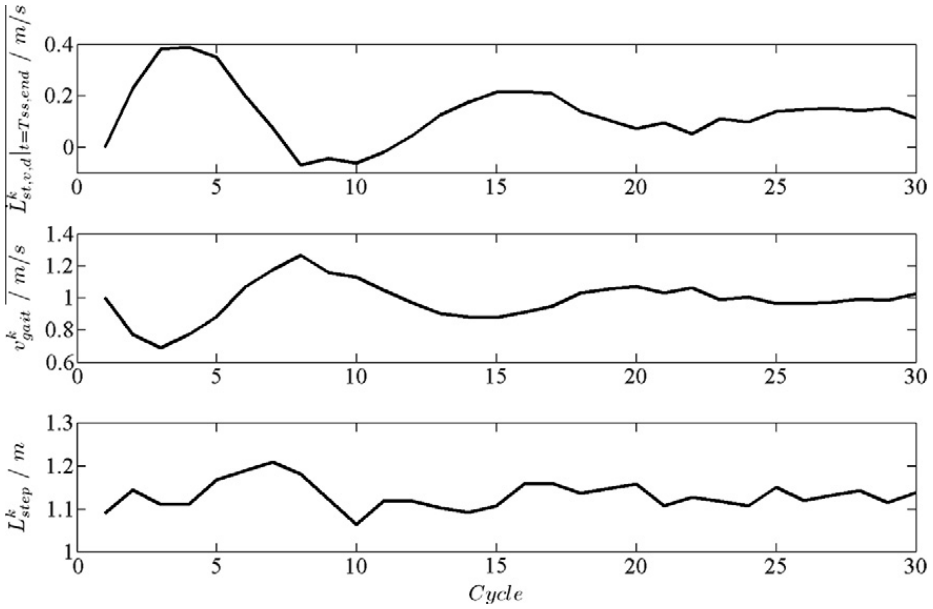

Fig. 8. A demonstrative performance of the proposed control strategy in Case 3.

shown in Fig. 8. We notice that considerable oscillations in $\dot{L}^k_{st,v,d}\big|_{t=T_{ss,end}}$, $v_{gait,d}$ and $L_{step,d}$ in first few gait cycles gradually decay until the actual gait velocity settles at expected desired gait velocity whereas the step length remains somewhat greater than desired.

The effect of $\dot{L}^k_{st,v,d}\big|_{t=T_{ss,end}}$ control reflects also in joint angles, torques and ground reaction forces (Fig. 9). While a correlation between $\dot{L}^k_{st,v,d}\big|_{t=T_{ss,end}}$ control and gait kinematics is not self-evident, in joint torque trajectories however one can observe a pronounced joint activity following a $\dot{L}^k_{st,v,d}\big|_{t=T_{ss,end}}$ increase and a decaying joint activity if $\dot{L}^k_{st,v,d}\big|_{t=T_{ss,end}}$ decreases which consequently leads to more pronounced peak values of vertical as well as horizontal ground reaction forces at the end of single support phase indicating more pronounced push off (for example, when comparing four successive ground reaction force peaks at the end of support phases – marked with arrows).

Particular walking parameter variations can also be addressed in terms of corresponding kinematic and kinetic characteristics. We will investigate them in terms of the following variables that correspond to generally adopted biomechanical nomenclature:

$$\begin{aligned} L_{Ankle\ angle} &= (q_{L,2} - q_{L,1})\tfrac{180^\circ}{pi} - 90^\circ \\ L_{Knee\ angle} &= (q_{L,2} - q_{L,3})\tfrac{180^\circ}{pi} \\ L_{Hip\ angle} &= (q_T - q_{L,3})\tfrac{180^\circ}{pi} \\ L_{Ankle\ moment} &= -T_{L,1} \\ L_{Knee\ moment} &= T_{L,2} \\ L_{Hip\ moment} &= T_{L,3} \end{aligned} \tag{33}$$

We will focus on one gait cycle, i.e. time interval between two consecutive impacts of the left leg, after the gait has settled. Note that due to non-infinitesimal integration step the exact time of contact nor time of take-off cannot be accurately determined. The first data sample of gait cycle is therefore the first data sample of double support which is at the most one integration step further in time with respect to the actual contact time. This reflects in somewhat different values as one would expect at the actual time of contact which would designate the beginning of gait cycle (for example non-zero ground reaction force at the beginning of gait cycle). However, if we consider gait as being a periodic process, the end of gait cycle may considered as time instance just before the contact.

Fig. 10 shows gait kinematics and kinetics in three simulation cases with different gait velocity. We notice that the range of ankle joint movement not only increased when gait was faster, but the joint angle trajectory gradually shifted towards greater ankle extension as well. Particularly well-defined is a rapid movement towards ankle extension peak value during push off and terminal stance in Case 2 and Case 3, whereas in Case 1 the joint dynamics was less explicit. In the knee joint trajectories we notice that the knee flexion at the beginning of the gait cycle and immediately after right leg contact decreases if gait velocity increases, whereas in the hip joint we recorded increasing extension joint pattern in the middle of the gait cycle. Similar patterns are present in joint moments. Ankle moment as well as knee moment trajectories displays gradually increasing behavior during push off that coincides with increasing gait velocity. On the other hand, increasing gait velocity has a minor effect on torso (less than 0.2°) and pelvis angle (less than 1°). Significant deviations between simulation

Author's personal copy

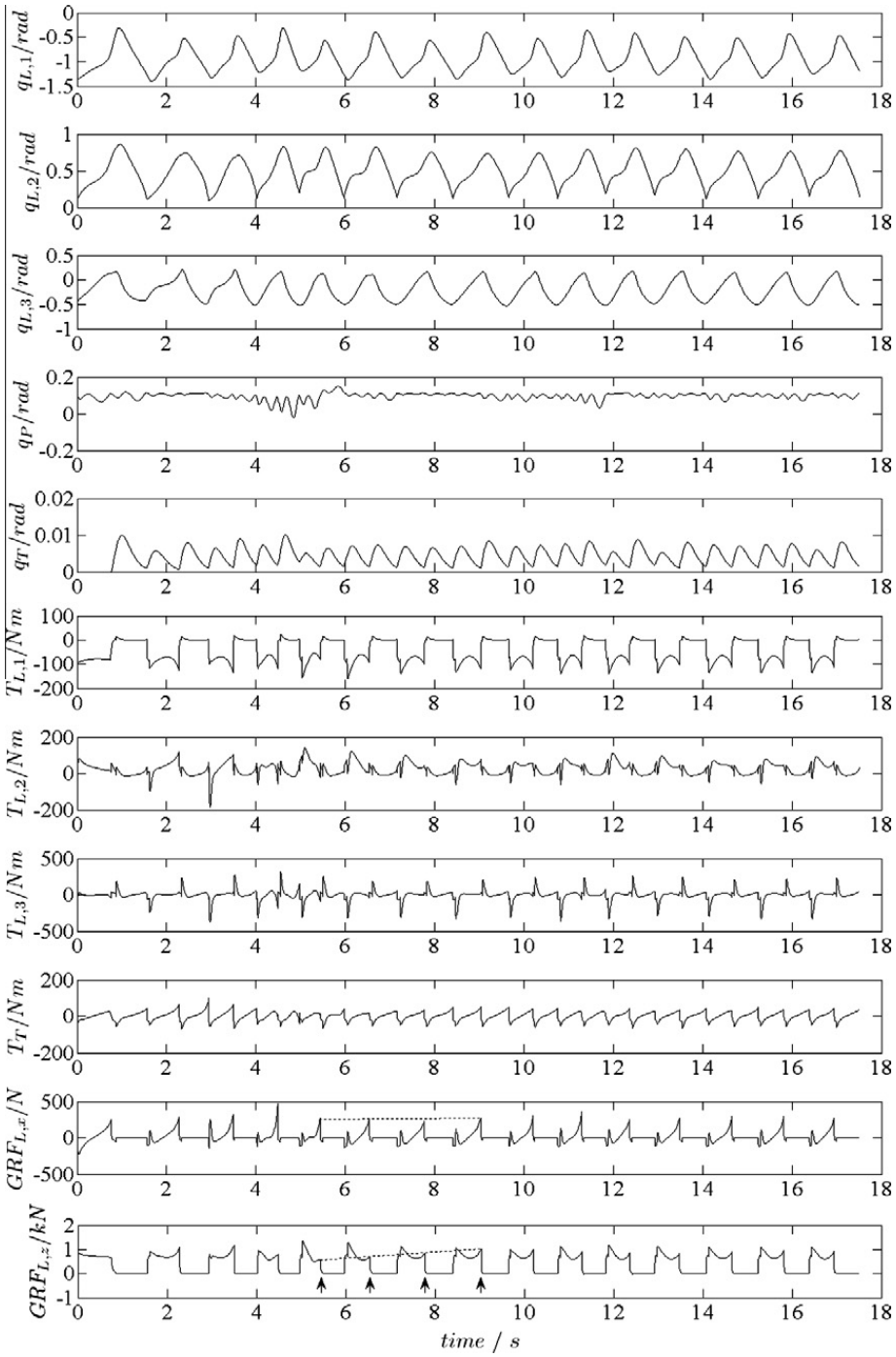

Fig. 9. Joint angles, torques and ground reaction forces for the left leg in Case 3.

cases are evident also in ground reaction forces where increasing gait velocity reflects in more pronounced horizontal as well as vertical ground reaction forces at push off.

Torso angle with respect to vertical is a very important aspect of human locomotion. The influence of torso angle on gait kinematics and kinetics was investigated in three simulation cases with different torso inclinations and is demonstrated in Fig. 11. We notice that the ankle flexion in midstance phase is most pronounced when the anterior inclination from vertical deviates the most (Case 5) and is less expressive when the torso segments remains at vertical position (Case 2). At the same time, increasing forward torso tilt reflects in increasing knee flexion pattern in midstance as well as in swing phase, whereas the magnitude of hip flexion in midstance is considerably higher only when torso inclined the most and does not deviates considerably in other simulation cases with less distinctive anterior tilt of the torso segment. Somewhat similar patterns are present in joint moments and ground reaction forces. On one hand ankle as well as knee moments display gradually increasing behavior of the extension moment during midstance that coincides with increasing torso angle, on the other hand a re-

Author's personal copy

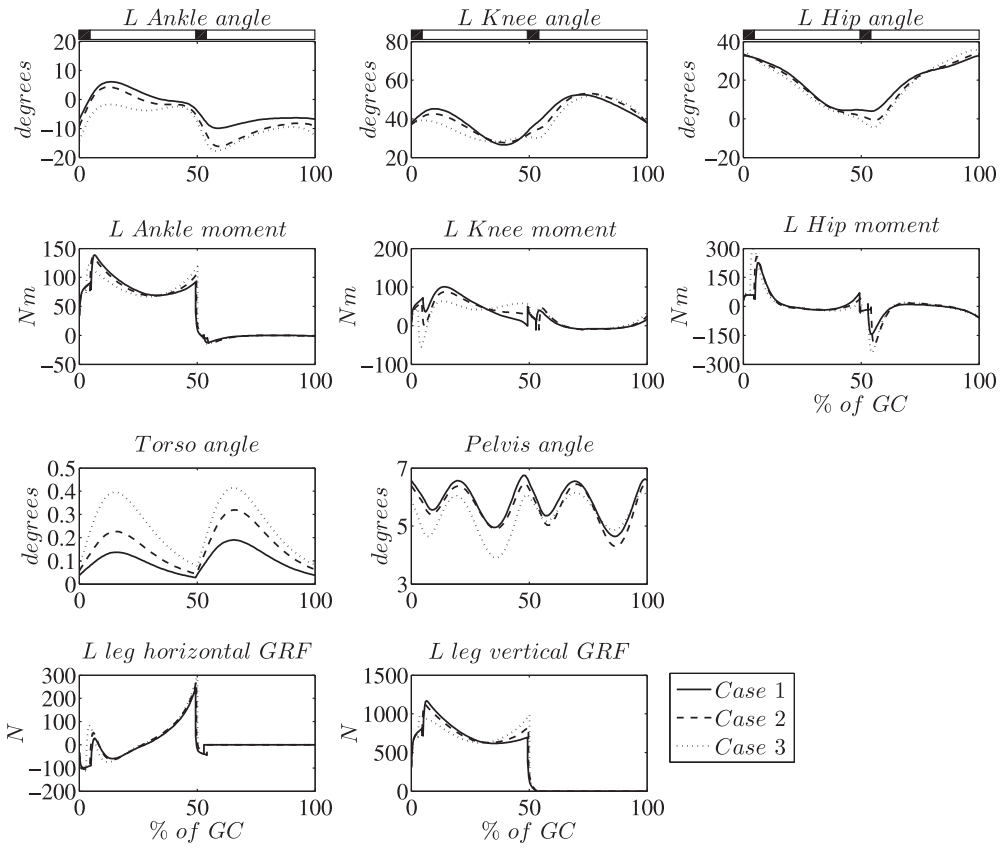

Fig. 10. Relation between gait velocity $v_{gait,d}$ and gait kinematics and kinetics. The sequence of black and white rectangles above the three graphs in the upper panel indicate consecutive phases of double support phase (0–5% of GC), left leg single support phase (5–50% of GC), double support phase (50–55% of GC) and left leg swing phase (55–100% of GC). Two transitions from black to white (5% of GC and 55% of GC) indicate right leg and left leg take-off respectively, whereas transition from white to black (50%) indicates the right leg contact phase. Additionally, the interval 0–10% of GC is referred to as early stance phase, the interval 10–40% is referred to as midstance, the push off indicates the interval 40–50% of GC and the interval 50–55% denotes terminal stance phase.

versed pattern is present during push off where vertical torso position is accompanied with most pronounced extension moment. Less significant are changes in pelvis angle, where the deviations between simulation cases do not exceed 1°. Vertical ground reaction forces exhibit similar behavior as ankle joint moment. In midstance vertical ground reaction force increases if torso angle increases whereas during push off a reversed pattern is evident – vertical ground reaction force increases if torso angle decreases.

Deviations in propulsion distribution profiles between ankle and knee joints are present predominantly in pathological gait where particular distribution profile reflects in unique kinematic and kinetic gait pattern. In our biped walking model we examined the influence of different propulsion distribution profiles by varying $\dot{L}_{st,ankle,v,d}$. Results are shown in Fig. 12. In Case 7 the maximal $\dot{L}_{st,ankle,v,d}$ leads to increased range of motion in ankle joint during push off and terminal phase, increased ankle extension at the beginning of the gait cycle as well as throughout the swing phase and somewhat greater flexion in midstance as opposed to considerably smaller range of motion, increased flexion at the beginning of the gait cycle and somewhat smaller flexion in midstance in Case 6 when $\dot{L}_{st,ankle,v,d}$ was the smallest. In the knee joint a reversed pattern is present. Case 7 exhibits substantially increased knee flexion early in the stance phase, terminal stance phase and throughout the swing phase and decreased knee flexion in midstance as compared to Case 2 or Case 6, where the knee joint angle peaks as well as joint range of motion gradually decreases according to $\dot{L}_{st,ankle,v,d}$. As opposed to ankle and knee joints, the deviations between simulation cases in hip joint trajectory are less pronounced and follow similar trends as in the knee joint. While there are no significant differences evident in the ankle joint moment, a distinctive knee extension moment deviations are evident in the knee joint. In Case 7 when $\dot{L}_{st,ankle,v,d}$ is the largest, we notice somewhat higher knee extension moment in midstance as in Case 2 and significantly increased in Case 6 when $\dot{L}_{st,ankle,v,d}$ is the smallest. During push off and terminal stance phase a reversed pattern is present; biped walking model exhibits the highest knee extension moment in Case 6, whereas in Case 7 the knee extension moment is reduced significantly. As in previous simulation sets, increasing $\dot{L}_{st,ankle,v,d}$ has only minor effect on torso and pelvis angle, i.e. less than 0.1° and 1° respectively. In ground reaction forces we notice somewhat decreased first peak in vertical component in Case 6, whereas in terminal stance and during push off we find both components of ground reaction force in Case 6 to be the largest.

Author's personal copy

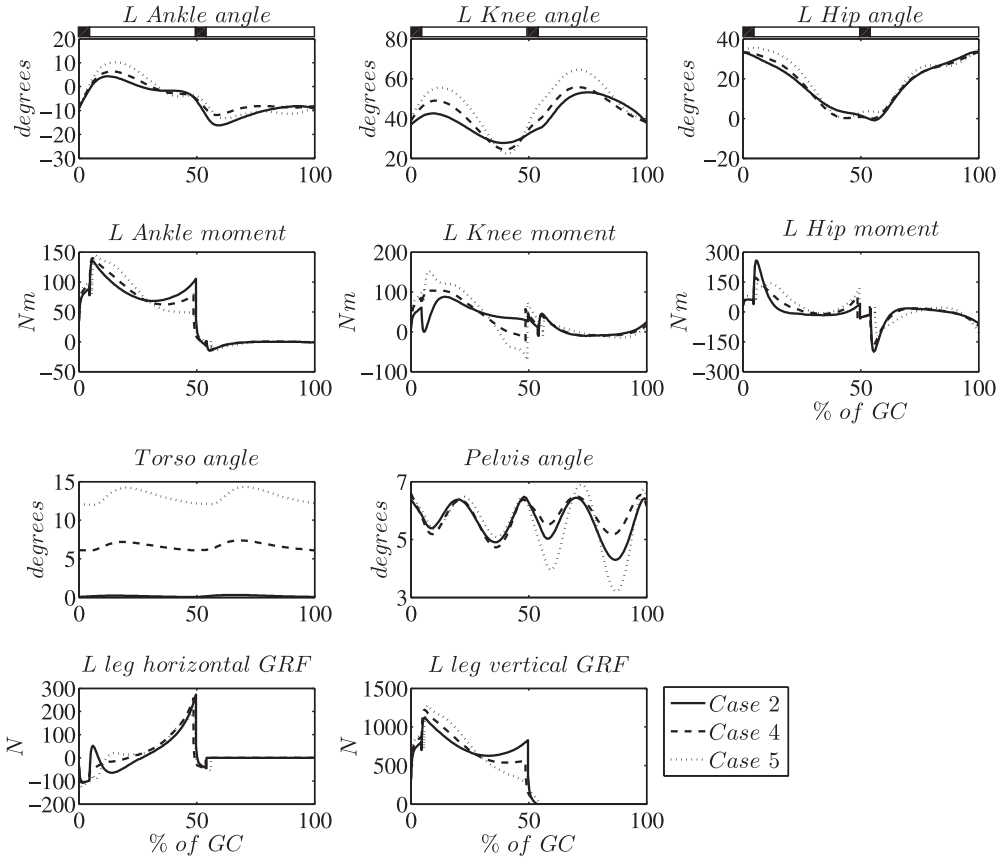

Fig. 11. Relation between torso angle $q_{T,d}$ and gait kinematics and kinetics.

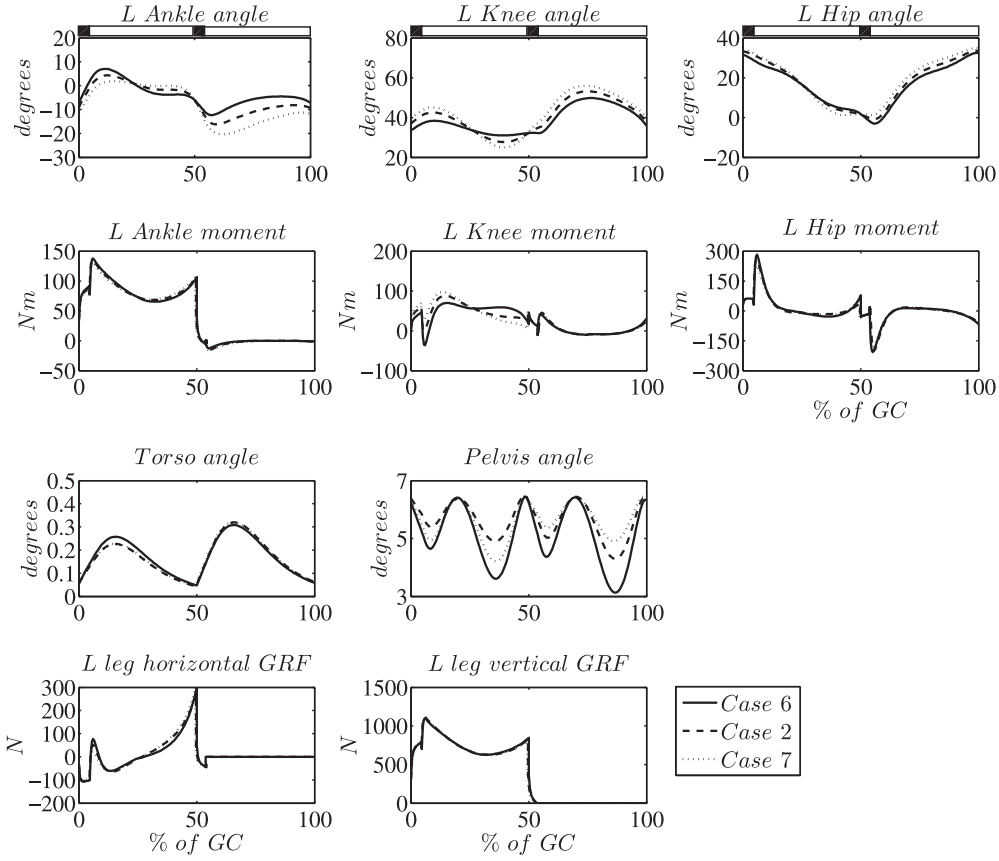

Fig. 12. Relation between lengthening velocity of the stance leg ankle component $\dot{L}_{st,ankle,v,d}$ and gait kinematics and kinetics.

Author's personal copy

6. Conclusion

Inspired by human locomotion this paper presents the concept of virtual leg that is controlled by two actuators and develops two-level control strategy for push off control in a 8 DOF biped walking model with non-instantaneous double to attain desired walking speed. The principle of push off is introduced by means of virtual stance leg lengthening velocity at the end of single support phase, which increases if walking speed is lower than desired and decreases if walking speed is higher than desired. Such push off mechanism and control imitates forceful extension of the trailing leg during push off in human locomotion and human gait velocity control strategy. The paper also demonstrates decomposition of virtual leg into ankle and knee components. Besides varying walking speed and torso angle, being able to vary propulsion distribution between ankle and knee joint present an important forward propulsion mechanism.

Simulation tests show that the proposed control strategy significantly improves the performance of the biped model and allows development of various walking modes for the biped walker at selected walking speeds, torso inclinations and propulsion distribution patterns even if the initial state of the model differs significantly from the settled values. Compared to similar models from the literature that develop stable walking in only certain walking condition and only when the gait starts sufficiently near the stable region, this may be considered a progress not only in biped robots and robot models but in the field of biomechanics as well. We believe that by extending the between-step control set of parameters from push off control to torso inclination and propulsion distribution profile adaptive control as well, we may be able in a biped walking model to some degree mimic a particular gait pattern. In this respect the present model lays a promising framework for future developments and applications of such models in the field of biomechanics as well.

References

[1] F.C. Anderson, M.G. Pandy, Dynamic optimization of human walking, J. Biomech. Eng. 231 (2001) 381–390.
[2] J.H. Choi, J.W. Grizzle, Feedback control of an underactuated planar bipedal robot with impulsive foot action, Robotica 23 (2005) 567–580.
[3] S. Collins, A. Ruina, R. Tedrake, M. Wisse, Efficient bipedal robots based on passive dynamic walkers, Sci. Mag. 307 (2005) 1082–1085.
[4] L.A. Gilchrist, D.A. Winter, A multisegment computer simulation of normal human gait, IEEE Trans. Rehabil. Eng. 5 (1997) 290–299.
[5] J.W. Grizzle, G. Abba, F. Plestan, Asymptotically stable walking for biped robots: analysis via systems with impulse effects, IEEE Trans. Autom. Contr. 46 (2001) 51–64.
[6] J.W. Grizzle, C.H. Moog, C. Chevallereau, Nonlinear control of mechanical systems with an unactuated cyclic variable, IEEE Trans. Autom. Contr. 30 (2005) 559–576.
[7] Y. Hurmuzlu, D.B. Marghitu, Rigid body collisions of planar kinematic chains with multiple contact points, Int. J. Robot. Res. 13 (1) (1994) 82–92.
[8] A. Isidori, Nonlinear Control Systems: An Introduction, second ed., Springer-Verlag, Berlin, Germany, 1989.
[9] A.D. Kuo, Energetics of actively powered locomotion using the simplest walking model, J. Biomech. Eng. 124 (2002) 113–120.
[10] R.Q. van der Linde, Design, analysis, and control of a low power joint for walking robots, by phasic activation of McKibben muscles, IEEE Trans. Robotic. Autom. 15 (1999) 595–604.
[11] R.Q. van der Linde, Passive bipedal walking with phasic muscle contraction, Biol. Cybern. 81 (1999) 227–237.
[12] T. McGeer, Passive dynamic walking, Int. J. Robot. Res. 8 (1990) 68–83.
[13] T. McGeer, Passive walking with knees, in: Proc. 1990 IEEE Robotics and Automation Conference, 1990, pp. 1640–1645.
[14] S. Miossec, J. Aoustin, A simplified stability for a biped walk with under and over actuated phases', Int. J. Robot. Res. 24 (7) (2005) 537–551.
[15] K. Mitobe, G. Capi, Y. Nasu, Control of walking robots based on manipulation of the zero moment point, Robotica 18 (2000) 651–657.
[16] S. Mochon, T.A. McMahon, Ballistic walking, J. Biomech. 13 (1980) 49–57.
[17] Xiuping Mu, Qiong Wu, Synthesis of a complete sagittal gait cycle for a five-link biped robot, Robotica 21 (2003) 581–587.
[18] A. Olenšek, Z. Matjačić, Human-like control strategy of a biped walking model, Robotica 26 (2008) 295–306.
[19] F. Plestan, J.W. Grizzle, E. Westervelt, G. Abba, Stable walking of a 7-DOF biped robot, IEEE Trans. Robotic. Autom. 19 (2003) 653–668.
[20] L. Roussel, C. Canudas-de-Wit, A. Goswami, Generation of energy optimal complete gait cycles for biped robots, in: Proc. IEEE International Conference on Robotics and Automation, Leuven, Belgium, 1998, pp. 2035–2041.
[21] M.W. Spong, F. Bullo, Controlled symmetries and passive walking, IEEE Trans. Autom. Contr. 50 (2005) 1025–1031.
[22] M. Vukobratovic, A.A. Frank, D. Juričić, On the stability of biped locomotion, IEEE Trans. Biomed. Eng. 17 (1970) 25–36.
[23] E.R. Westervelt, J.W. Grizzle, Design of asymptotically stable walking for a 5-link planar biped walker via optimization, in: Proc. IEEE International Conference on Robotics and Automation, Washington, DC, USA, 2002, pp. 3117–3122.
[24] E.R. Westervelt, J.W. Grizzle, D.E. Koditschek, Hybrid zero dynamics of planar biped walkers, IEEE Trans. Autom. Contr. 48 (2003) 42–56.
[25] D.A. Winter, Energy generation and absorption at the ankle and knee during fast, natural, and slow cadences, Clin. Orthop. Relat. Res. 175 (1983) 147–154.
[26] D.A. Winter, Biomechanical motor patterns in normal walking, J. Motor. Behav. 15 (1983) 302–330.
[27] M. Wisse, A.L. Schwab, F.C.T. van der Helm, Passive dynamic walking model with upper body, Robotica 22 (2004) 681–688.
[28] F.E. Zajac, R.R. Neptune, S.A. Kautz, Biomechanics and muscle coordination of human walking Part I: introduction to concepts, power transfer, dynamics and simulations, Gait Posture 16 (2002) 215–232.
[29] F.E. Zajac, R.R. Neptune, S.A. Kautz, Biomechanics and muscle coordination of human walking Part II: Lessons from dynamical simulations and clinical implications, Gait Posture 17 (2003) 1–17.
[30] E.R. Westervelt, J.W. Grizzle, C. Canudas de Wit, Switching and PI control of walking motions of planar biped walkers, IEEE Trans. Autom. Contr. 48 (2) (2003) 308–312.
[31] J.W. Grizzle, E.R. Westervelt, C. Canudas-de-Wit, Event-based PI control of an underactuated biped walker, in: Proc. IEEE Conference on Decision and Control, December 2003.